# Experimental and Computational Studies of the Kinetics of the Reaction of Atomic Hydrogen with Methanethiol

Katherine E. Kerr, Ionut M. Alecu, Kristopher M. Thompson, Yide Gao, and Paul Marshall*

Department of Chemistry and Center for Advanced Scientific Computing and Modeling, University of North Texas, 1155 Union Circle #305070, Denton, Texas 76203-5017, United States

Ⓢ Supporting Information

ABSTRACT: The overall rate constant for $H + CH_3SH$ has been studied over 296–1007 K in an Ar bath gas using the laser flash photolysis method at 193 nm. H atoms were generated from CH_3SH and in some cases NH_3. They were detected via time-resolved resonance fluorescence. The results are summarized as $k = (3.45 \pm 0.19) \times 10^{-11}$ cm^3 molecule^{-1} s^{-1} exp(-6.92 ± 0.16 kJ mol$^{-1}/RT$) where the errors in the Arrhenius parameters are the statistical uncertainties at the 2σ level. Overall error limits of $\pm 9\%$ for k are proposed. In the overlapping temperature range there is very good agreement with the resonance fluorescence measurements of Wine et al. *Ab initio* data and transition state theory yield moderate accord with the total rate constant, but not with prior mass spectrometry measurements of the main product channels leading to $CH_3S + H_2$ and $CH_3 + H_2S$ by Amano et al.
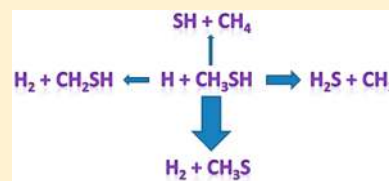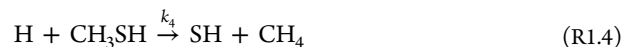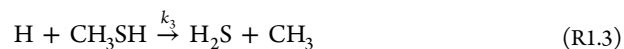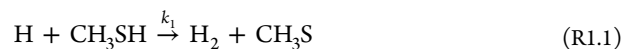
1. INTRODUCTION

Organosulfur compounds contribute to the chemistry of a number of systems, including emissions from plankton into the atmosphere,[1] the Claus process for removing sulfur from hydrocarbon fuels,[2] and chemical vapor deposition of diamond films.[3] Here we focus on one of the simplest compounds, methanethiol, and its bimolecular reaction with atomic hydrogen

$$H + CH_3SH \xrightarrow{k} products \qquad (R1)$$
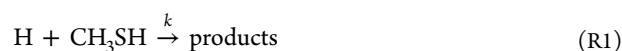
The total H atom removal rate constant k has been studied before, most notably by Wine et al.[4] over 247–405 K at total bath gas pressures in the range 50–76 Torr (1 Torr ≈ 1.33 mbar) using the resonance fluorescence flash photolysis technique with 248 nm laser pulses, and by Amano et al.[5] over 313–454 K at pressures between 250 and 290 Torr using an electron beam and mass spectrometry. The previous work has found the reaction to be second-order, with no pressure dependence observed over the narrow ranges studied. Rate constants from the two studies do not agree and, as will be seen, our experiments support those of Wine et al. The reaction has also been studied at room temperature.[6-9] One aim of the present work is to increase the temperature range to beyond 1000 K, which results in data now being available over a factor of 4 range in temperature. These data prove challenging to model theoretically, in part because the properties of the dominant transition state are constrained by comparison with experiment over a wide range of collision energies.

An intriguing aspect of this reaction is that there are several thermochemically plausible channels. These include H atom abstraction from the SH group (R1.1), H atom abstraction from the CH_3 group (R1.2), breaking the C–S bond and displacing the CH_3 group (R1.3), and cleavage of the C–S bond and displacing the SH group (R1.4):

$$H + CH_3SH \xrightarrow{k_1} H_2 + CH_3S \qquad (R1.1)$$

$$H + CH_3SH \xrightarrow{k_2} H_2 + CH_2SH \qquad (R1.2)$$

$$H + CH_3SH \xrightarrow{k_3} H_2S + CH_3 \qquad (R1.3)$$

$$H + CH_3SH \xrightarrow{k_4} SH + CH_4 \qquad (R1.4)$$

The thermochemistry of these pathways is summarized in Table 1. High-accuracy enthalpies of formation are available for H, CH_3, and CH_4 from the Active Thermochemical Tables[10] and for H_2S, CH_3SH, and CH_3S from the NIST Computational

Table 1. Thermochemistry and Barrier Heights of Possible Reaction Channels for the $H + CH_3SH$ Reaction at 0 K

product channel	experimental $\Delta_r H_0$/ kJ mol^{-1} [a]	computed $\Delta_r H_0$/kJ mol^{-1} [b]	computed $E_{b_0}^{\ddagger}$/kJ mol^{-1} [b]
$H_2 + CH_3S$ (1)	−74.29	−73.33	8.17
$H_2 + CH_2SH$ (2)		−39.71	36.91
$H_2S + CH_3$ (3)	−71.95	−72.80	14.40
$SH + CH_4$ (4)	−128.12	−128.86	81.09

[a] See text. [b] Via a modified W1 method (see text).

Chemistry Comparison and Benchmark Database,[11] and we have previously recommended thermochemistry for SH.[12] Another aim of the work is to investigate the product branching ratios by computational methods. There has been an initial theoretical study of three of these channels by Wang et al., who employed G3(MP2) energies and deduced that channel R1.1 was the major pathway.[13] Channel R1.4, which is the most exothermic pathway, has not been considered previously. Here we modify the W1U algorithm of Martin and co-workers[14] to investigate the transition states and derive the rate constants k_1-k_4. We also make a detailed analysis of the roles of anharmonicity in the reactants and transition states. Our theoretical data are compared to the measurements of channels R1.1 and R1.3 by Amano et al. as well as the present measurements, and the Wine et al. results for the total rate constant $k = \Sigma k_i$. Theoretical expressions for $k_1 - k_4$ are derived for temperatures up to 3000 K. Although CH_3SH will be short-lived at high temperatures, these expressions combined with the known equilibrium constants will assist modeling of sulfur systems via the reverse of processes R1.1−R1.4, in analysis of situations where reactions of species such as SH and CH_3S are relevant, for example, CS_2 formation in the Claus process[15] and the oxidation of H_2S/CH_4 mixtures in the combustion of sour gas.[16,17]

2. EXPERIMENTAL METHODOLOGY

We applied the flash photolysis/resonance fluorescence method. Our apparatus and its operation have been described elsewhere,[18−20] including modifications for studying atomic hydrogen.[21,22] Here the hydrogen atoms were generated by pulsed excimer laser photolysis of precursor molecules at a wavelength of 193 nm. Slow flows of the precursors were diluted in a large excess of inert Ar bath gas to maintain isothermal conditions, monitored with a retractable thermocouple corrected for radiation errors, and to slow diffusion of radicals to the walls of the reactor. Methanethiol itself can photolyze via two pathways, breaking either the S−H bond or the C−S bond:

$$CH_3SH + h\nu \rightarrow CH_3S + H \qquad (R2.1)$$

$$CH_3SH + h\nu \rightarrow CH_3 + SH \qquad (R2.2)$$
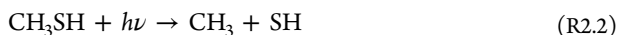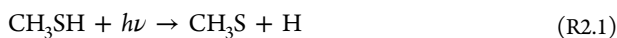
The bond dissociation energies have been measured as 385 ± 4 kJ mol^{-1} for the S−H bond and 314 ± 6 kJ mol^{-1} for the C−S bond.[23] The branching to the second pathway was measured to be 7% by Bridges and White at 248 nm and is more significant at shorter wavelengths.[24] At lower temperatures we used photolysis of a small fraction of the methanethiol reactant itself as the hydrogen source, with photolysis energies kept low to minimize the initial radical concentrations. At higher temperatures it became difficult to generate enough H atoms to observe the reaction without causing excessive secondary chemistry. Ammonia was used instead, and the reaction was checked at lower temperatures to verify agreement with the methanethiol-sourced points. Ammonia has a larger absorption cross section at 193 nm than methanethiol. Initial photolytic H atom concentrations were estimated separately from the laser pulse energy, E, the cross-sectional area of the laser beam of 0.50 cm^2 and the absorption cross-section, σ, which is 5.0×10^{-18} cm^2 for ammonia[25] and 1.86×10^{-18} cm^2 for CH_3SH.[26] The quantum yield of H from ammonia is taken to be 1, and to be 0.55 for CH_3SH.[26]

Resonance fluorescence was excited by a microwave plasma in a flowing sample of diluted H_2, which generated Lyman α radiation at 122 nm. Magnesium fluoride optics were employed,

and a dry air filter helped isolate the Lyman α wavelength from other atomic lines which might be present. Fluorescence signals were captured with a solar blind photomultiplier tube and processed through a pulse discriminator, and photon counts as a function of time were accumulated for typically several hundred decays (repeated at ∼1 Hz) in a multichannel scaler.

Once formed, H atoms are removed through two main pathways, reaction R1 and diffusion out of the observation zone, which is described by an effectively first-order rate constant k_{diff}. The corresponding rate expression is

$$\frac{d[H]}{dt} = -k[H][CH_3SH] - k_{diff}[H] = -k_{ps1}[H] \qquad (1)$$

We employed $[CH_3SH] \gg [H]$, so the change in $[CH_3SH]$ will be negligible over the course of the reaction. Under these pseudo-first-order conditions k_{ps1} is the pseudo-first-order rate constant. We therefore expect $[H]$ to decay exponentially. The observed hydrogen atom fluorescence signal I_f was fit to a single-exponential function of time t, where A and B are constants:

$$I_f = Ae^{-k_{ps1}t} + B \qquad (2)$$

The constant B accounts for a constant background in the signal, caused primarily by constant scattered light from the resonance lamp. An example time profile of I_f is shown as the inset in Figure 1. The exponential decays are fitted with a nonlinear least-
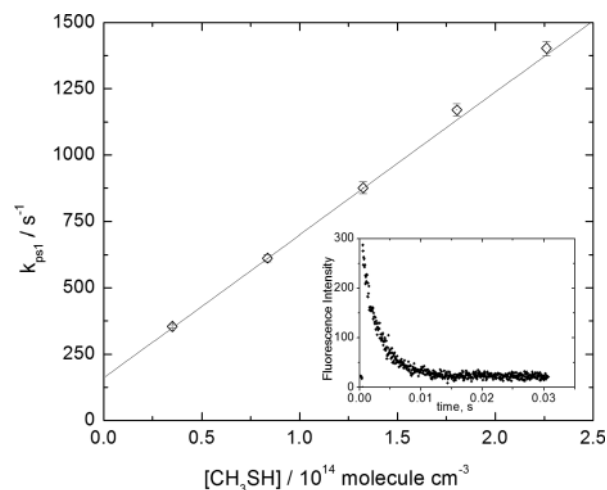
Figure 1. Determination of the second-order rate constant k by plotting k_{ps1} with 2σ error bars obtained from each pseudo-first-order decay against $[CH_3SH]$. The inset shows the decay from the first k_{ps1} point. In this experiment, at 450 K and 67 mbar, CH_3SH was the only hydrogen atom source.

squares fitting algorithm that yields k_{ps1} and its statistical error.[27,28] Variation of $[CH_3SH]$ allows k to be separated from diffusion effects, and k is obtained as the slope of plots of k_{ps1} vs $[CH_3SH]$ like that shown in Figure 1. Weighted linear least-squares fits to the k_{ps1} vs $[CH_3SH]$ plots, which take into account the horizontal and vertical error bars, are used to determine the second-order rate constant k, along with its statistical 1σ error.

3. EXPERIMENTAL RESULTS

Table 2 summarizes 35 determinations of k, each from five different methanethiol concentrations, with the largest value tabulated. Apart from changing the temperature T, we emphasized variation of the experimental parameters τ, the average residence time inside the heated reactor before

Table 2. Experimental Conditions and Measured Rate Constants k for the H + CH₃SH Reaction

T/K	τ/s	$F/\text{mJ cm}^{-2}$	p/mbar	$[CH_3SH]_{max}/10^{14}\text{cm}^{-3}$ molecule	$[NH_3]/10^{14}\text{cm}^{-3}$ molecule	$k/10^{-12}\text{ cm}^3$ molecule^{-1} s^{-1}	$[H]_{0,max}/10^{11}\text{ cm}^{-3}$ molecule	$[Ar]/10^{17}\text{ cm}^{-3}$ molecule
290	1.5	0.34	26.7	15.2	0	1.83 ± 0.16	5.1	6.6
295	3.7	1.49	66.7	14.7	0	1.83 ± 0.27	22	16.3
295	3.7	0.99	66.5	14.7	0	1.81 ± 0.15	14	16.3
296	2.9	1.14	133.5	17.6	0	2.15 ± 0.10	20	32.7
296	3.7	2.42	66.8	11.0	0	1.97 ± 0.09	26	16.4
296	1.3	0.45	69.1	2.1	4.0	2.12 ± 0.06	9.7	16.9
296	1.3	0.22	69.1	2.1	4.0	2.04 ± 0.06	4.7	16.9
299	1.2	0.20	68.1	2.3	3.8	2.22 ± 0.09	4.1	16.5
299	1.2	0.09	68.1	2.3	3.8	2.15 ± 0.09	1.9	16.5
447	1.2	1.58	66.5	1.5	0	5.79 ± 0.28	2.4	10.8
448	2.5	3.50	66.7	4.7	0	5.97 ± 0.38	16	10.8
449	2.5	2.08	66.7	3.5	0	5.38 ± 0.07	7.2	10.7
449	2.5	1.34	66.7	3.5	0	5.34 ± 0.05	4.7	10.7
449	2.5	0.65	66.7	3.5	0	5.31 ± 0.34	2.3	10.7
600	0.4	0.08	65.7	1.1	5.4	10.3 ± 0.39	2.3	7.9
601	0.7	0.30	26.7	1.4	4.4	8.34 ± 0.33	6.8	3.2
601	0.7	0.09	26.7	1.4	4.4	7.11 ± 0.25	2.2	3.2
601	0.9	0.09	66.7	1.6	1.7	8.57 ± 0.17	0.93	8.0
601	0.9	0.05	66.7	1.6	1.7	8.84 ± 0.49	0.45	8.0
605	0.7	0.03	26.7	0.8	1.7	7.23 ± 0.61	0.29	3.2
605	0.7	0.07	26.7	0.8	1.7	7.39 ± 0.57	0.68	3.2
605	0.4	0.08	27.9	1.0	3.9	10.5 ± 0.31	1.6	3.3
795	0.7	0.12	66.4	2.0	9.9	11.2 ± 0.8	6.0	6.0
795	0.7	0.07	66.4	2.0	9.9	11.1 ± 0.5	3.7	6.0
797	0.1	0.44	13.6	0.9	2.0	11.7 ± 1.1	4.7	1.2
800	0.3	0.32	27.7	1.0	2.5	11.0 ± 0.7	4.2	2.5
801	0.3	0.30	30.1	1.8	2.5	10.2 ± 1.5	4.1	2.7
802	0.3	0.29	14.1	1.0	2.8	11.3 ± 0.8	4.3	1.3
806	0.3	0.52	27.3	1.3	2.6	12.7 ± 0.4	7.2	2.5
806	0.3	0.22	27.3	1.3	2.6	12.2 ± 0.7	3.1	2.5
806	0.7	0.13	70.3	0.8	11.0	10.6 ± 1.6	7.2	6.3
806	0.7	0.06	70.3	0.8	11.0	10.6 ± 0.7	3.5	6.3
1002	0.08	0.07	15.7	0.6	2.4	17.0 ± 1.4	0.88	1.1
1005	0.15	0.08	13.5	0.5	3.0	16.4 ± 1.5	1.2	1.0
1014	0.11	0.08	13.9	0.3	3.0	16.1 ± 2.0	1.2	1.0

photolysis, and the total pressure p, which check for good mixing and the lack of thermal decomposition within the reactor. The laser fluence F and the precursor concentrations control the initial radical concentrations and were adjusted to ensure that exponential decays of [H] were seen. The maximum estimated initial H atom concentration of course increases along with [CH₃SH]. In this regime no systematic variation of k with the experimental parameters was noted, so that reaction R1 appears to have been isolated from secondary chemistry involving photolysis or reaction products.

The data are plotted in Arrhenius form in Figure 2 and may be summarized over 296−1007 K as

$$k = (3.45 \pm 0.19) \times 10^{-11} \text{ cm}^3 \text{ molecule}^{-1} \text{ s}^{-1}$$
$$\times \exp(-6.92 \pm 0.16 \text{kJmol}^{-1}/RT) \tag{3}$$

where the errors in the Arrhenius parameters are the statistical uncertainties at the 2σ level. Bearing in mind possible systematic errors, we propose overall error limits of ±9% in k.

Our measurements agree very well with those of Wine et al.[4] in the overlapping temperature region, as shown in Figure 2, as do their reported Arrhenius parameters of $(3.45 \pm 0.14) \times 10^{-11}$ cm³ molecule⁻¹ s⁻¹ and 7.03 ± 0.07 kJ mol⁻¹. Comparison with the total rate constant from Amano et al.[5] indicates agreement

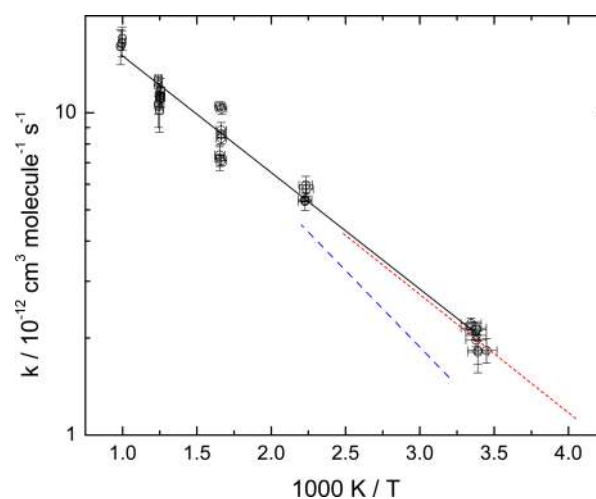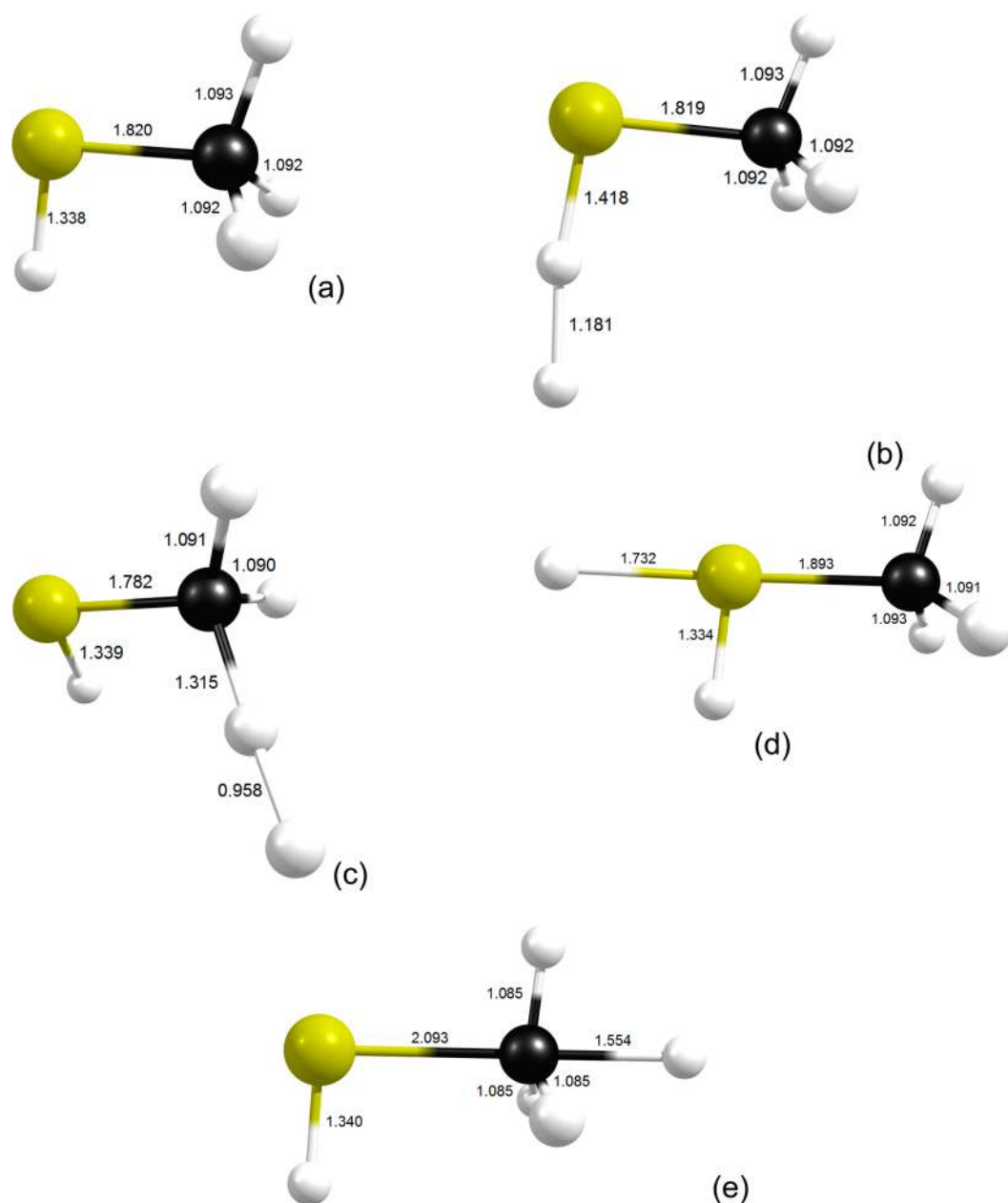**Figure 2.** Arrhenius plot of the present measurements for the total H + CH₃SH rate constant, with 1σ error bars in k and T. Also shown is previous work by Wine et al.,[4] short red dashes, and Amano et al.,[5] blue dashes.

only to within a factor of 2−3, a larger deviation than expected from the statistical uncertainties alone. In units of 10^{-12} cm³

Figure 3. Structures derived with QCISD/6-311G(d,p) theory for (a) methanethiol and (b)−(e) transition states TS1−4 for its reactions with hydrogen atoms via pathways R1.1−R1.4.

molecule^{-1} s^{-1}, at room temperature Vaghjiani et al.[6] and Martin et al.[7] found k equal to 2.13 ± 0.31 and 2.19 ± 0.20 whereas we obtain 2.11 ± 0.18. Balla and Heicklen[8,9] derived values of k_1 for channel R1.1 of around 4.07 × 10^{-13} and 1.79 × 10^{-12} cm^3 molecule^{-1} s^{-1} by fitting to complex mechanisms involving H + NO and H + O$_2$, respectively. The latter value appears to be more accurate. Overall, our results agree with most of the prior measurements and extend the temperature range to over 1000 K.

4. COMPUTATIONAL ANALYSIS

4.1. Potential Energy Diagram. *Ab initio* methods were applied to the stationary points of the H + CH$_3$SH reaction. The geometries and vibrational frequencies (the latter scaled by a standard factor of 0.954[11]) were obtained using QCISD/6-311G(d,p) theory.[29,30] This scaling factor accounts for the typically modest anharmonicity in most vibrations, so that the computed harmonic frequencies are scaled to match observed v = 0 → v = 1 fundamental transitions. A more detailed approach is outlined below for certain highly anharmonic normal modes. These QCISD geometries are used for single-point energies derived via the W1U methodology of Martin and co-workers,[14] to yield coupled cluster energies CCSD(T) extrapolated to the infinite basis set limit along with corrections for core electron correlation and scalar relativistic effects. This is a modification of the original W1U method, which was based on density functional theory for the geometry and frequencies. The absolute energies obtained in this way are summarized in the Supporting Information (Table S1). These *ab initio* calculations were made with the GAUSSIAN 09 program suite.[31] An empirical correction of −2.255 kJ mol^{-1} is applied to the energy of the SH radical to account for the spin−orbit splitting of its $^2\Pi$ state.[11] The corresponding reaction enthalpies are compared with

experiment in Table 1, and the accord is seen to be very good, with a root-mean-square deviation of only 0.9 kJ mol^{-1}. This same level of theory was applied to the transition states (TSs) of reactions R1.1−R1.4 which are illustrated in Figure 3. The complete geometries and other details are provided in the Supporting Information (Table S2). The resulting barrier heights at 0 K, including zero-point vibrational energy, are listed in Table 1 and the four reaction pathways are sketched in the potential energy diagram of Figure 4. It may be seen that the thermochemistry of the different pathways is an incomplete guide to the ordering of the energy barriers.
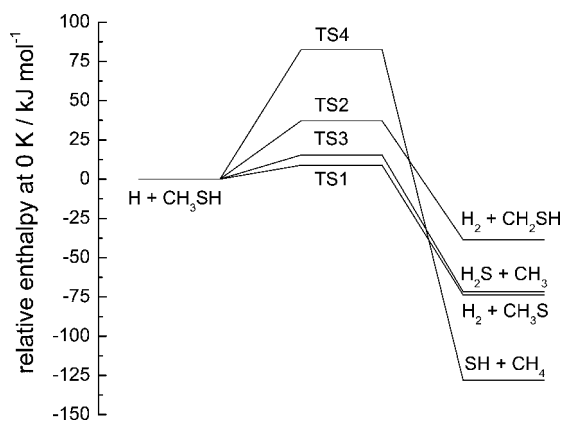

Figure 4. Potential energy diagram for H + CH$_3$SH based on modified W1U theory (see text).

4.2. Simple Kinetic Analysis. Simply looking at the barriers suggests that channels R1.2 and R1.4 will make only small contributions to the overall rate constant k, and that channels R1.1 to R1.3 will be the two dominant pathways. Amano et al.[5] focused their mass spectrometric experiments on these latter two pathways and obtained $k_1 = 4.8 \times 10^{-11}$ cm^3 molecule^{-1} s^{-1} exp(-10.9 kJ mol$^{-1}/RT$) and $k_3 = 1.15 \times 10^{-11}$ cm^3 molecule^{-1} s^{-1} exp(-7.0 kJ mol$^{-1}/RT$). For a quantitative comparison we evaluate canonical variational transition state theory (usually abbreviated to CVT)[32] for the four channels over 200−3000 K, using the implementation of Truhlar and co-workers in POLYRATE.[33] The CVT calculations also account for the effects of multidimensional tunneling on the rate constants for channels R1.1−R1.4 via the small curvature tunneling (SCT) approximation.[34] Reaction coordinates were characterized using QCISD/6-311G(d,p) theory and the resulting classical barriers (i.e., exclusive of zero-point vibrational energy) were scaled to match the modified W1U values with zero point energy stripped out. GAUSSRATE was used to interface with the GAUSSIAN code to execute *ab initio* computations in the course of each kinetic run.[35] The methodology is detailed elsewhere;[33] here we provide the input files in the Supporting Information to enable reproduction of the CVT/SCT analysis. These calculations relied on all the normal modes being treated as harmonic oscillators. Of course, methanethiol and the transition states contain methyl rotors.

4.3. Roles of Anharmonicity and Symmetry. We developed a torsion correction factor τ^F to take into account the effects of anharmonicity in modes like the internal rotors, where the harmonic oscillator model will give unrealistic partition functions. First, the energy changes along each torsional mode were evaluated using relaxed scans (i.e., the rest of the geometry was allowed to reoptimize) as a function of torsion angle, at the QCISD/6-311G(d,p) level of theory. For the

bimolecular transition states the lengths of the forming and breaking bonds were held fixed in this exercise. The results are shown in Figure 5. To discuss methanethiol as an example, a straightforward treatment might be to recognize the three symmetrical minima with an internal rotation symmetry number $\sigma_{IR} = 3$ and to obtain an approximate potential by assuming a sinusoidal form and fitting to the harmonic frequency at the bottom of the well (ν_{tors}), σ_{IR}, and the moment of inertia for twisting (assumed not to change significantly during torsion). This latter quantity was obtained with the MOMINERT algorithm within the MULTWELL suite of Barker and co-workers.[36] Figure 5a shows this would be a reasonable procedure for methanethiol. The torsional potential also controls the reaction path degeneracy, which we denote as RPD. This has been carefully discussed elsewhere,[37,38] with the conclusion that RPD = $m^{\dagger}\sigma/m\sigma^{\dagger}$. For a given species, σ is the product of the overall rotational symmetry number (obtained easily via group theory) and the internal rotation symmetry number (which is not always obvious; complications can arise if there are wells are of different depths), † denotes a transition state rather than reactant property, and m is the number of optical isomers if the species is chiral. Two limiting cases for developing partition functions of torsions can be identified. If the barrier is very high (relative to k_BT), then the system's behavior tends toward that of a set of σ_{IR} harmonic oscillators. If there are no barriers (and no minima), then a free rotor partition function can be defined analytically as $(\pi k_BT/hB)^{1/2}$ (with the moment of inertia B in Hz), which does not include a σ_{IR} factor. Of course many systems, including all those here, fall in between. In some cases a species is chiral, and its enantiomers may be interconvertable by a torsion or a bend. In the former case, two distinct enantiomers may contribute to the count of σ_{IR}. If the bending frequency is high, then there are two distinguishable harmonic oscillators, accounted for by $m = 2$, and if it corresponds to a transition state, then the reaction flux passes independently through one transition state and its mirror image. In the limit as the separating barrier tends to zero, we effectively tend toward a single structure.

Questions can arise such as what are the appropriate values of m and σ_{IR} and where do these variables "go" as k_BT becomes larger than the barriers to torsion or bending? Sophisticated methods exist to address these issues, and we have recently applied an example, the MS-T approach of Truhlar and co-workers,[39] to the behavior of N$_2$O$_5$, which contains two coupled internal rotors.[40] However, the systems here are simpler and contain a single torsion that we assume is separable from the other motions of the molecules. We explore the direct numerical solution of the Schrödinger equation for the anharmonic modes with the help of the FGH program,[41] and from the energy levels obtained, ε_i, deduce the anharmonic partition q_{anh} by direct summation of the Boltzmann terms, $q_{anh} = \Sigma\exp(-\varepsilon_i/k_BT)$. We defined our zero such that $\varepsilon_0 = 0$. This procedure naturally accounts for the number of minima, whether they are equally deep or not, and whether levels are split significantly by tunneling, and it does not require an analytic form of the potential. We interpolated 240 points, with a spline fit, for the potentials shown in Figure 5, and computed the first 80 eigenvalues ε_i. As may be seen, most species have a simple potential like that for methanethiol. Typical aspects are that bound levels near the bottom of the well are almost triply degenerate (they are split by a few wavenumbers because of mixing via tunneling between the minima), there is complex behavior at energies around the top of the barrier, and at high energies quasi-degenerate pairs of energy levels are found, which
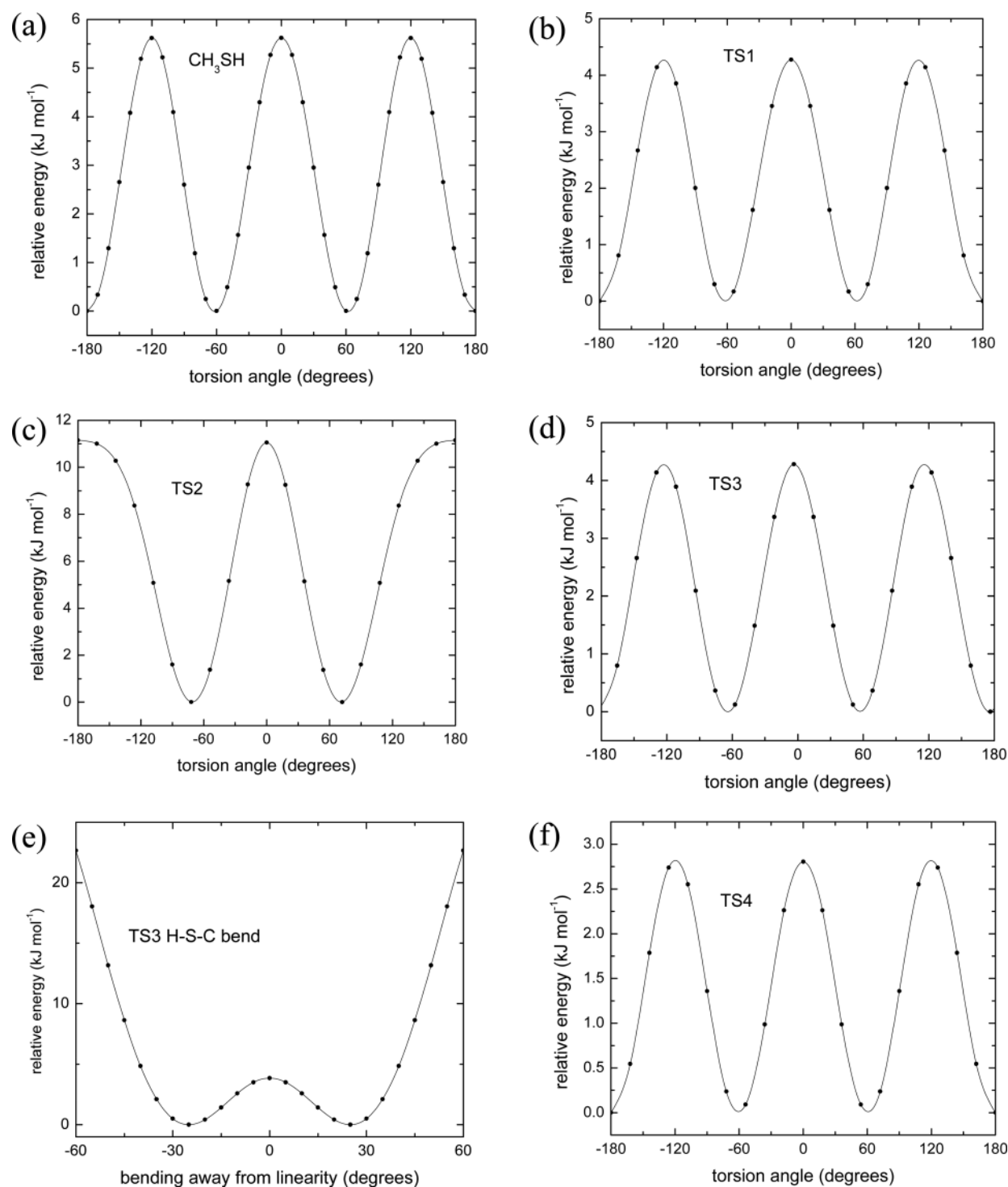
Figure 5. Anharmonic potentials from relaxed scans at the QCISD/6-311G(d,p) level of theory: (a) C−S torsion in methanethiol, (b) C−S torsion in TS1; (c) C−S torsion in TS2; (d) C−S torsion in TS3; (e) H−S−C bending in TS3; (f) C−S torsion in TS4.

correspond to positive and negative angular momentum for free rotor states. Because the lower levels have ε comparable to $k_B T$, the overall free rotor partition function is not a good approximation until very high temperatures in our system.

4.4. Kinetic Results. Given that the underlying CVT/SCT rate constant calculations were performed with all modes treated as harmonic vibrations, we multiply the rate constant by a factor $\tau^F(\text{TS})/\tau^F(\text{reactant})$, which allows both for anharmonicity and the reaction path degeneracy and for transition between the

limiting cases noted above. τ^F is defined as $q_{\text{anh}}/q_{\text{harm}}$, where q_{harm} is obtained on the same basis as q_{anh}, so here it is $(1 - \exp(-h\upsilon_{\text{tors}}/k_B T))^{-1}$. For pathway R1.1, although both CH$_3$SH and TS1 showed major deviations from the harmonic oscillator model, these deviations were by similar factors and so mostly cancel when they combine in the final rate constant. Much the same occurs for pathway R1.4 and the torsional contribution to R1.3. TS2 is an example of a chiral species, whose enantiomers interconvert by internal rotation around the C−S bond. We had

initially speculated whether to allow for internal rotational symmetry for each of the two enantiomers; inspection of the corresponding potential in Figure 5 shows this would be a mistake. In fact, similar transition states were encountered in cases involving radical attacks on the methyl group in methanol[42−44] and, as discussed in those instances, in these situations one must be careful not to double-count the torsional contribution. Because a torsional treatment based on the potential for internal rotation leading to the interconversion between the two distinguishable (nonsuperposable) minima already captures the contributions of each of these, the subsequent inclusion of a chirality factor is superfluous. TS3 is also chiral. We allow for torsion around the C−S bond in the usual way, but this torsion does not transform one enantiomer to the other. Instead, this interconversion is accomplished by an H−S−C bending mode. We mapped out part of this double-well potential in Figure 5 and solved for that motion too to arrive at a second τ^F factor. All the τ^F results are summarized in Table 3. The

Table 3. Anharmonicity Correction Factors $\tau^F = q_{anh}/q_{harm}$ Computed Directly from the QCISD/6-311G(d,p) Potentials

T/K	torsion in CH_3SH	torsion in TS1	torsion in TS2	torsion in TS3	bending in TS3	torsion in TS4
200	3.15	3.18	2.06	3.24	2.02	3.31
250	3.23	3.21	2.10	3.30	2.07	3.31
298.15	3.29	3.22	2.14	3.32	2.10	3.27
300	3.29	3.22	2.14	3.32	2.10	3.27
400	3.33	3.18	2.23	3.31	2.12	3.16
600	3.29	3.02	2.38	3.16	2.10	2.91
800	3.17	2.84	2.46	2.99	2.04	2.68
1000	3.04	2.68	2.49	2.83	1.96	2.50
1200	2.91	2.54	2.49	2.68	1.88	2.34
1500	2.74	2.35	2.45	2.49	1.76	2.15
1800	2.59	2.20	2.39	2.34	1.64	2.00
2000	2.50	2.12	2.35	2.25	1.57	1.92
2400	2.34	1.97	2.27	2.10	1.43	1.78
3000	2.15	1.80	2.14	1.91	1.27	1.61

CVT/SCT kinetic results are listed in Table 4, and summaries in the form of modified Arrhenius expressions (of the form $k = AT^n \exp(-B/T)$) are provided in Table 5. These are shown graphically on Figure 6.

This figure illustrates some of the limitations of our kinetic analysis. Perhaps the most striking aspect is that all the theoretical

lines are distinctly curved, with n for the two dominant channels in the range 1−2, as would be expected on the basis of the likely temperature dependence of the partition functions.[45] By contrast, the combined experimental data set over 250−1000 K clearly is consistent with n near 0. This must limit the possibilities for any close agreement between theory and experiment.

Considering initially the overall rate constant, we can see that the behavior of eq 3 is reproduced to within a factor of 3 or better. At first sight this might be called "good", although systematic deviations are apparent. At temperatures above the Pauling point of around 650 K, CVT/SCT yields k that is too high and has a local activation energy (defined via the slope) that is too high. By contrast, at below around 500 K CVT/SCT is low by roughly a factor of 2. One hopes that a more sophisticated analysis could resolve some of these discrepancies. If the experimental data were available only over a small range of temperature, the strategies of further scaling the transition state frequencies (which affects the extent of looseness in the TS, i.e., the entropy and thus the pre-exponential A factor) and/or correcting the TS energy (i.e., altering the slope of the Arrheius plot) could be applied to reduce discrepancies between theory and experiment. However, with our new measurements spanning a wide range of $1/T$, improving the fit at one end of the range worsens the accord at the other. We speculate that more complex factors, such as the extent of quantum mechanical tunneling, may need to be considered in greater depth.

There are significant disagreements concerning the product branching ratios. Along with Wang et al.,[13] we find a major role for channel R1.1 (H abstraction from the SH group) and a small role for channel R1.3 (formation of $CH_3 + H_2S$). At 298 and 1000 K our CVTST yields 95% and 81%, respectively, for the contribution of channel R1.1. At 1000 K there is an 18% contribution by channel R1.3 and a 1.5% contribution from channel R1.2 (H abstraction from the CH_3 group), whereas channel R1.4 (formation of $SH + CH_4$) is negligible (0.5%) even at 2000 K. By contrast, the experiments by Amano et al.[5] yielded much larger branching ratios of 52% and 40% for channel R1.3 at 313 and 454 K, respectively. Further experiments might help to resolve this disagreement. We note that if the computed barrier heights were allowed to vary by, e.g., around 1 kcal mol^{-1}, then there would be a significant impact on the computed branching ratios, potentially of the order of a factor of 4 at 400 K. However, the errors in the computed reaction enthalpies shown in Table 1,

Table 4. Rate Constants for H + CH$_3$SH Obtained via SCT/CVTST Theory with Corrections for Anharmonicity

T/K	k_1	k_2	k_3	k_4	total k
200	1.84×10^{-13}	5.85×10^{-19}	2.06×10^{-15}	6.04×10^{-28}	1.86×10^{-13}
250	4.41×10^{-13}	6.11×10^{-18}	1.23×10^{-14}	3.30×10^{-26}	4.53×10^{-13}
298.15	8.29×10^{-13}	3.72×10^{-17}	4.03×10^{-14}	1.78×10^{-24}	8.69×10^{-13}
300	8.47×10^{-13}	3.95×10^{-17}	4.19×10^{-14}	2.07×10^{-24}	8.88×10^{-13}
400	2.13×10^{-12}	6.02×10^{-16}	2.01×10^{-13}	1.62×10^{-21}	2.34×10^{-12}
600	6.47×10^{-12}	1.58×10^{-14}	1.06×10^{-12}	3.28×10^{-18}	7.54×10^{-12}
800	1.29×10^{-11}	1.10×10^{-13}	2.60×10^{-12}	1.95×10^{-16}	1.56×10^{-11}
1000	2.14×10^{-11}	4.05×10^{-13}	4.65×10^{-12}	2.53×10^{-15}	2.65×10^{-11}
1200	3.20×10^{-11}	1.06×10^{-12}	7.04×10^{-12}	1.48×10^{-14}	4.01×10^{-11}
1500	5.13×10^{-11}	3.02×10^{-12}	1.10×10^{-11}	9.33×10^{-14}	6.54×10^{-11}
1800	7.46×10^{-11}	6.50×10^{-12}	1.51×10^{-11}	3.35×10^{-13}	9.66×10^{-11}
2000	9.22×10^{-11}	9.81×10^{-12}	1.79×10^{-11}	6.49×10^{-13}	1.21×10^{-10}
2400	1.32×10^{-10}	1.90×10^{-11}	2.34×10^{-11}	1.82×10^{-12}	1.76×10^{-10}
3000	2.01×10^{-10}	3.93×10^{-11}	3.14×10^{-11}	5.39×10^{-12}	2.77×10^{-10}

Table 5. Summary of Computed Kinetics in Modified Arrhenius Form, $k = A(T/K)^n \exp(-BK/T)$ cm^3 molecule^{-1} s^{-1}

reaction	A	n	B	valid T range/K
H + CH$_3$SH → H$_2$ + CH$_3$S (1)	2.30×10^{-16}	1.729	496	200–3000
H + CH$_3$SH → H$_2$ + CH$_2$SH (2)	6.91×10^{-21}	2.925	2389	250–3000
H + CH$_3$SH → CH$_3$ + H$_2$S (3)	1.19×10^{-13}	0.766	1623	200–3000
H + CH$_3$SH → CH$_4$ + SH (4)	1.16×10^{-17}	1.983	8321	400–3000
H + CH$_3$SH → products	1.49×10^{-16}	1.824	509	200–3000
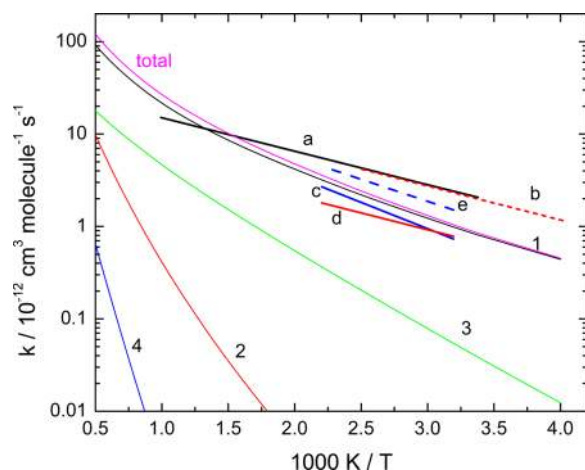
Figure 6. Arrhenius plot of rate constants for H + CH$_3$SH. Experimental data are shown in heavy lines and transition state theory results in narrow lines. The labels 1−4 refer to channels R1.1−R1.4, and "total" is the overall rate constant. Experimental data are (a) this work, total; (b) ref 4, total; (c) ref 5 for channel R1.1; (d) ref 5 for channel R1.3; (e) ref 5, combined.

of up to 1 kJ mol^{-1}, are consistent with the idea of subkcal mol^{-1} accuracy for the saddle points too.

5. CONCLUSIONS

The Arrhenius relation determined by Wine et al. for the overall rate constant of H + CH$_3$SH is found to extend to ∼1000 K. Four exothermic product channels have been characterized via *ab initio* methods. The thermochemistry is well-reproduced and the magnitude of the overall rate constant is computed to within about a factor of 2 with canonical variational transition state theory, the small-curvature tunneling model and a detailed treatment of certain anharmonic modes. The channel leading to H$_2$ + CH$_3$S is predicted to be the dominant pathway, by contrast to the study by Amano et al., who found roughly equal branching to CH$_3$ + H$_2$S.

■ ASSOCIATED CONTENT

ⓢ Supporting Information

Complete geometrical parameters, modified W1U energies, and vibrational frequencies for the reactants, transition states, and products for reactions R1.1−R1.4 optimized at the QCISD/6-311G(d,p) level of theory, and input data for transition state theory. This material is available free of charge via the Internet at http://pubs.acs.org.

■ AUTHOR INFORMATION

Corresponding Author

*P. Marshall. E-mail: marshall@unt.edu.

Notes

The authors declare no competing financial interest.

■ ACKNOWLEDGMENTS

■ REFERENCES

(1) Bates, T. S.; Lamb, B. K.; Guenther, A.; Dignon, J.; Stoiber, R. E. Sulfur Emissions to the Atmosphere from Natural Sources. *J. Atm. Chem.* **1992**, *14*, 315−337.

(2) Gargurevich, I. A. Hydrogen Sulfide Combustion: Relevant Issues under Claus Furnace Conditions. *Ind. Eng. Chem. Res.* **2005**, *44*, 7706−7729.

(3) Petherbridge, J. R.; May, P. W.; Shallcross, D. E.; Harvey, J. N.; Fuge, G. M.; Rosser, K. N.; Ashfold, M. N. R. Simulation of H-C-S Containing Gas Mixtures Relevant to Diamond Chemical Vapor Deposition. *Diamond Relat. Mater.* **2003**, *12*, 2178−2185.

(4) Wine, P. H.; Nicovich, J. M.; Hynes, A. J.; Wells, J. R. CH$_3$SH Photolysis at 248 nm. Hydrogen Atom Yield and Rate Constant for the H + CH$_3$SH Reaction. *J. Phys. Chem.* **1986**, *90*, 4033−4037.

(5) Amano, A.; Yamada, M.; Hashimoto, K.; Sugiura, K. Kinetic Feature of the Reaction Between Methanethiol and Hydrogen Atoms. *Nippon Kagaku Kaishi* **1983**, *3*, 385−393.

(6) Vaghjiani, G. L.; Ravishankara, A. R. Photodissociation of H$_2$O$_2$ and CH$_3$OOH at 248 nm and 298 K: Quantum Yields for OH, O(^{3}P) and H(^{2}S). *J. Chem. Phys.* **1990**, *92*, 996−1003.

(7) Martin, D.; Jourdain, J. L.; Le Bras, G. Kinetics and Mechanism for the Reactions of H Atoms with CH$_3$SH and C$_2$H$_5$SH. *Int. J. Chem. Kinet.* **1988**, *20*, 897−907.

(8) Balla, R. J.; Heicklen, J. Oxidation of Sulfur Compounds. IV. The Photo-Oxidation of CH$_3$SH. *J. Photochem.* **1985**, *29*, 311−332.

(9) Balla, R. J.; Heicklen, J. Oxidation of Sulfur Compounds. I. The Photolysis of CH$_3$SH and (CH$_3$S)$_2$ in the Presence of NO. *Can. J. Chem.* **1984**, *62*, 162−170.

(10) Ruscic, B. *Active Thermochemical Tables*, version 1.112; Argonne National Laboratory: Lemont, IL, http://atct.anl.gov (accessed Aug 14, 2014).

(11) *NIST Computational Chemistry Comparison and Benchmark Database*, Release 16a; Johnson, R. D., III, Ed.; 2013; http://cccbdb.nist.gov/.

(12) Peebles, L. R.; Marshall, P. High-Accuracy Coupled-Cluster Computations of Bond Dissociation Energies in SH, H$_2$S and H$_2$O. *J. Chem. Phys.* **2002**, *117*, 3132−3138.

(13) Wang, Y.-X.; Duan, X.-M.; Wang, Q.; Liu, J.-Y. Direct Ab Initio Dynamics on the Reaction of Methanethiol and Hydrogen Atom. *Acta Phys. Chim. Sin.* **2010**, *26*, 183−187.

(14) Barnes, E. C.; Petersson, G. A.; Montgomery, J. A., Jr.; Frisch, M. J.; Martin, J. M. L. Unrestricted Coupled Cluster and Brueckner Doubles Variations of W1 Theory. *J. Chem. Theory Comput.* **2009**, *5*, 2687−2693.

(15) Karan, K.; Behie, L. A. CS$_2$ Formation in the Claus Reaction Furnace: A Kinetic Study of Methane-Sulfur and Methane-Hydrogen Sulfide Reactions. *Ind. Eng. Chem. Res.* **2004**, *43*, 3304−3313.

(16) Selim, H.; Al Shoaibi, A.; Gupta, A. K. Fate of Sulfur with H$_2$S Injection in Methane/Air Flames. *Appl. Energy* **2012**, *92*, 57−64.

(17) Bongartz, D.; Ghoniem, A. F. Chemical Kinetics Mechanism for Oxy-Fuel Combustion of Mixtures of Hydrogen Sulfide and Methane. *Combust. Flame* **2015**, *162*, 544−553.

(18) Ding, L.; Marshall, P. Kinetic Studies of the Reactions of Atomic Chlorine and Bromine with Silane. *J. Phys. Chem.* **1992**, *96*, 2197−2201.

(19) Goumri, A.; Laakso, D.; Rocha, J.-D. R.; Francis, E.; Marshall, P. An Investigation of the Gas-Phase Kinetics of the Reaction K + SO$_2$ + Ar. *J. Phys. Chem.* **1993**, *97*, 5295−5297.

(20) Alecu, I. M.; Gao, Y.; Hsieh, P.-C.; Sand, J. P.; Ors, A.; McLeod, A.; Marshall, P. Studies of the Kinetics and Thermochemistry of the Forward and Reverse Reaction Cl + C$_6$H$_6$ = HCl + C$_6$H$_5$. *J. Phys. Chem. A* **2007**, *111*, 3970−3976.

(21) Peng, J.; Hu, X.; Marshall, P. Experimental and ab Initio Investigations of the Kinetics of the Reaction of H Atoms with H$_2$S. *J. Phys. Chem. A* **1999**, *103*, 5307−5311.

(22) Gao, Y.; DeYonker, N. J.; Garrett, E. C.; Wilson, A. K.; Cundari, T. R.; Marshall, P. Enthalpy of Formation of the Cyclohexadienyl Radical and the C−H Bond Enthalpy of 1,4-Cyclohexadiene: An Experimental and Computational Re-Evaluation. *J. Phys. Chem. A* **2009**, *113*, 6955−6963.

(23) Benson, S. W. Thermochemistry and Kinetics of Sulfur-Containing Molecules and Radicals. *Chem. Rev.* **1977**, *78*, 23−35.

(24) Bridges, L.; White, J. M. Photochemistry of Methanethiol at 254 and 214 nm. *J. Phys. Chem.* **1973**, *77*, 295−298.

(25) Chen, F. Z.; Judge, D. L.; Wu, C. Y. R.; Caldwell, J. Low and Room Temperature Photoabsorption Cross Sections of NH$_3$ in the UV Region. *Planetary Space Sci.* **1998**, *47*, 261−266.

(26) Barone, S. B.; Turnipseed, A. A.; Gierczak, T.; Ravishankara, A. R. Quantum Yields of H(^{2}S) and CH$_3$S(^{2}E) from the Photolysis of Simple Organosulfur Compounds at 193, 222, and 248 nm. *J. Phys. Chem.* **1994**, *98*, 11969−11977.

(27) Marshall, P. Method for Analyzing Exponential Decays. *Comput. Chem.* **1987**, *11*, 219−221.

(28) Marshall, P. Errata. *Comput. Chem.* **1989**, *13*, 103.

(29) McLean, A. D.; Chandler, G. S. Contracted Gaussian-Basis Sets for Molecular Calculations. 1. 2nd Row Atoms, Z=11−18. *J. Chem. Phys.* **1980**, *72*, 5639−5648.

(30) Hehre, W. J.; Radom, L.; Schleyer, P. v. R.; Pople, J. A. *Ab Initio Molecular Orbital Theory*; Wiley: New York, 1986.

(31) Frisch, M. J.; Trucks, G. W.; Schlegel, H. B.; Scuseria, G. E.; Robb, M. A.; Cheeseman, J. R.; Scalmani, G.; Barone, V.; Mennucci, B.; Petersson, G. A.; et al. *Gaussian 09*; Gaussian Inc.: Wallingford, CT, 2009.

(32) Garrett, B. C.; Truhlar, D. G. Variational Transition-State Theory. *Acc. Chem. Res.* **1980**, *13*, 440−448.

(33) Zheng, J.; Zhang, S.; Lynch, B. J.; Corchado, J. C.; Chuang, Y.-Y.; Fast, P. L.; Hu, W.-P.; Liu, Y.-P.; Lynch, G. C.; Nguyen, K. A.; et al. *POLYRATE: Computer Program for the Calculation of Chemical Rates for Polyatomics*, version 2010-A; University of Minnesota: Minneapolis, MN, 2010.

(34) Liu, Y.-P.; Lynch, G. C.; Truong, T. N.; Lu, D.-h.; Truhlar, D. G. Molecular Modeling of the Kinetic Isotope Effect for the [1,5]-Sigmatropic Rearrangement of cis-1,3-Pentadiene. *J. Am. Chem. Soc.* **1993**, *115*, 2408−2415.

(35) Zheng, J.; Zhang, S.; Corchado, J. C.; Chuang, Y.-Y.; Coitino, E. L.; Ellingson, B. A.; Truhlar, D. G. *GAUSSRATE*, version 2009-A; University of Minnesota: Minneapolis, MN, 2009.

(36) Barker, J. R.; Ortiz, N. F.; Preses, J. M.; Lohr, L. L.; Maranzana, A.; Stimac, P. J.; Nguyen, L. T.; Kumar, T. J. D. *MultiWell-2014.1*, 2014, http://aoss-research.engin.umich.edu/multiwell/.

(37) Gilbert, R. G.; Smith, S. C. *Theory of Unimolecular and Recombination Reactions*; Oxford University Press: Oxford, U.K., 1990.

(38) Fernandez-Ramos, A.; Ellingson, B. A.; Meana-Paneda, R.; Marques, J.; Truhlar, D. G. Symmetry Numbers and Chemical Reaction Rates. *Theor. Chem. Acc.* **2007**, *118*, 813−826.

(39) Zheng, J.; Yu, T.; Papajak, E.; Alecu, I. M.; Mielke, S. L.; Truhlar, D. G. Practical Methods for Including Torsional Anharmonicity in Thermochemical Calculations on Complex Molecules: The Internal-Coordinate Multi-Structural Approximation. *Phys. Chem. Chem. Phys.* **2011**, *13*, 10885−10907.

(40) Alecu, I. M.; Marshall, P. Computational Study of the Thermochemistry of N$_2$O$_5$ and the Kinetics of the Reaction N$_2$O$_5$ + H$_2$O → 2 HNO$_3$. *J. Phys. Chem. A* **2014**, *118*, 11405−11416.

(41) Johnson, R. D., III. Fourier Grid Hamiltonian 1D Program, ver 1.01 http://www.nist.gov/mml/csd/informatics_research/fourier_grid_hamiltonian_interface.cfm, 1999.

(42) Chuang, Y.-Y.; Radhakrishnan, M. L.; Fast, P. L.; Cramer, C. J.; Truhlar, D. G. Direct Dynamics for Free Radical Kinetics in Solution: Solvent Effect on the Rate Constant for the Reaction of Methanol with Atomic Hydrogen. *J. Phys. Chem. A* **1999**, *103*, 4893−4909.

(43) Meaña-Paneda, R.; Truhlar, D. G.; Fernández-Ramos, A. High-Level Direct-Dynamics Variational Transition State Theory Calculations Including Multidimensional Tunneling of the Thermal Rate Constants, Branching Ratios, and Kinetic Isotope Effects of the Hydrogen Abstraction Reactions from Methanol by Atomic Hydrogen. *J. Chem. Phys.* **2011**, *134*, 094302.

(44) Alecu, I. M.; Truhlar, D. G. Computational Study of the Reactions of Methanol with the Hydroperoxyl and Methyl Radicals. 2. Accurate Thermal Rate Constants. *J. Phys. Chem. A* **2011**, *115*, 14599−14611.

(45) Mulcahy, M. F. R. *Gas Kinetics*; Nelson: London, 1973.